# A Three-color Coupled Level-Set Algorithm for Simultaneous Multiple Cell Segmentation and Tracking

Jierong Cheng, Wei Xiong, Ying Gu, Shue-Ching Chia, Yue Wang, and Joo-Hwee Lim

Institute for Infocomm Research, 1 Fusionopolis Way, #21-01 Connexis (South Tower), Singapore 138632

**Abstract.** High content computational analysis of time-lapse microscopic cell images requires accurate and efficient segmentation and tracking. In this work, we introduce "3LS", an algorithm using only three level sets to segment and track arbitrary number of cells in time-lapse microscopic images. The cell number and positions are determined in the first frame by extracting concave points and fitting ellipses after initial segmentation. We construct a graph representing cells and the background with vertices and their adjacency relationships with edges. Each vertex of the graph is assigned with a color tag by applying a vertex coloring algorithm. In this way, the boundary of each cell can be embedded in one of three level set functions. The "3LS" algorithm is implemented in an existing coupled active contour framework (nLS) [1] to handle overlapped cells during segmentation. However, we improve nLS using a new volume conservation constraint (VCC) to prevent shrinkage or expansion on whole cell boundaries and produce more accurate segmentation and tracking of touching cells. When tested on four different time-lapse image sequences, the 3LS outperforms the original nLS and other relevant state-of-the-art counterparts in both segmentation and tracking however with a notable reduction in computational time.

## 1 Introduction

High throughput microscopy provides an unprecedented opportunity to visualize cellular events at high resolutions over time. Time-resolved microscopic imaging has become popular in studying basic cellular processes such as motility, migration, deformation, population dynamics, etc. However, increasing quantity of images of high throughput readouts coupled with complexity of the underlying information makes manual analysis of such images prohibitive.

Commercial microscopy software packages generally feature tools for object segmentation and tracking [2]. However, simple intensity based thresholding fails for cells observed in nonfluorescent imaging modes and for cells in contact. Likewise, standard correlation matching cannot keep track of cells that change their shapes. Such limitations are often partly compensated by graphical user interfaces that allow users to manually correct processing errors, but at the expense of speed and reproducibility – the main benefits of automation.

Existing cell tracking methods can be divided into two main classes. Algorithms in the first class perform cell detection and linking between cells from different frames separately. The linking process is usually based on certain criteria of the similarities in spatial positions and appearance of the cells. A typical method is "favorite matching" through a distance matrix computed from the Euclidean distance of the cell centroids and the sizes [3–5]. In [6], a dissimilarity measure was designed based on the spatial distribution, nuclei morphological appearance, migration, and intensity information. In [7], the similarities were calculated from object center coordinates, size, and total intensity. For tracking of mitotic cell nuclei, object correspondences were determined by searching for trajectories with maximum smoothness [8]. A framework combining mean shift and Kalman filters was designed for cell tracking [9]. The main difficulty of this type of methods is to split or merge the tracks in the event when the total number of objects is changed.

Algorithms in the second class integrate cell segmentation and tracking in a model evolution approach [2]. Mostly based on active contours or deformable models, they extend from segmentation to tracking by using the extracted contours of objects in the previous frame as initialization for the segmentation of the current frame. In [10], a parametric active contour based method was presented for the tracking of cell migrations in microscopy videos. Due to the inability of parametric contours to handle cell interactions, topological operators had to be introduced to handle cell divisions. In addition, the concept of repulsive contours were proposed to handle cell contact. It is notable that the initialization of the parametric active contours must be done manually on the first frame of the temporal sequence. Geometric active contour approaches based on level sets neither require any explicit parameterization nor suffer from any constraints on the topology. Such approaches have been used for segmenting and tracking cells in 2D images [11–14] and dynamic 3D images [1, 15]. The main disadvantage of the model evolution approaches is the computational cost: to prevent cell fusion, each cell $i$ has to be represented by its own level set function $\phi_i$; a pair-wise coupling constraint is introduced to prevent neighbouring contours from overlapping each other (the details can be found in Section 2.1). Hence, if an image contains $N$ cells, $N$ level set functions $\phi_i, i = 1, 2, ..., N$ will be needed and the number of such coupling constraint terms will be $N^2$.

To reduce the number of level set functions representing multiple objects, vertex coloring has been proposed in a four-color level set algorithm [16] where a graph is constructed with vertices used for representing cells and edges used for their adjacency relationships. It is noted that, in all existing relevant approaches, the image background is not represented explicitly. In the present work, we choose to represent each background explicitly with a fixed vertex in the graph. With these concepts in mind, we introduce our 3LS algorithm which uses only three level set functions to tackle the problem of segmenting and tracking multiple cells simultaneously.

Besides cell overlapping in microscopic images, cells of similar intensity levels may touch and this causes errors in level set based cell tracking. To handle

this, Dufour introduced a volume conservation constraint (VCC) term in his algorithms presented in [1]. However, the VCC term results in shrinkage or expansion on whole cell boundary. To avoid this undesirable effect, we introduce an improved VCC and combine it with a pair-wise coupling term. With these modifications, we propose a three-color coupled level set algorithm for the segmentation and tracking of arbitrary number of cells in time-lapse microscopic images with overlapping and touching cells. Notably, the proposed algorithm can reduce computational costs significantly while achieving better segmentation and tracking accuracy. This is validated by our numerical experiments.

## 2 Related work

### 2.1 N-coupled level sets

The tracking algorithms using coupled implicit active contours [11]/surfaces [1] are an extension to Chan and Vese's two-phase model in the level-set framework [17]. In order to track each cell separately, one level set function $\phi_i$ is assigned to each cell, $i = 1, 2, .., n$. In the 2D model, the total energy function for the $n$ level sets (nLS) is given by

$$E(\phi_1, ..., \phi_n, c_O, c_{I,1}, ..., c_{I,n}) = \iint_\Omega \sum_{i=1}^{n} \Bigg[ \alpha\delta(\phi_i)|\nabla\phi_i| + \lambda_I H(\phi_i)(I - c_{I,i})^2 + \frac{\lambda_O}{n} \prod_j (1 - H(\phi_j)) (I - c_O)^2 + \gamma \sum_{i<j} H(\phi_i)H(\phi_j) \Bigg] dxdy + \frac{1}{2} \sum_{i=1}^{n} \eta_i \left( \iint_\Omega H(\phi_i)dxdy - V_i^0 \right)^2 \quad (1)$$

In this expression, $c_{I,i}$ and $c_O$ are the mean intensity of voxels inside the $i$th level set $\phi_i$ and outside all the current level sets respectively. $\delta(\phi)$ and $H(\phi)$ are the Dirac and Heaviside functions, respectively. $I = I(x, y)$ is the image intensity at $(x, y) \in \Omega, \Omega \subset \mathbb{R}^2$. The term weighted by $\gamma$ penalizes the pair-wise overlaps between distinct contours. The last term is the volume (or area in 2D) conservation constraint (VCC) introduced in [1] by Dufour which helps to improve the segmentation of touching cells. $V_i^0 = \iint_\Omega H(\phi_i^0)dxdy$ is the volume of cell $i$ segmented from the first frame. When cells of similar intensity levels touch, the image dependent terms (the first three terms) are insufficient to determine the boundary between cells correctly. Without the VCC, the active contour evolution will depend primarily on the initialization and result in one contour engulfing the other contour.

From Eq. (1), for each $\phi_i$, one can derive a time $t$ indexed surface evaluation equation as follows:

$$\frac{\partial \phi_i}{\partial t} = \Bigg[\alpha \nabla \cdot \frac{\nabla \phi_i}{|\nabla \phi_i|} - \lambda_I (I - c_{I,i})^2 + \lambda_O \prod_{j \neq i} (1 - H(\phi_j)) (I - c_O)^2 - \gamma \sum_{j \neq i} H(\phi_j) - \eta_i \left( \iint_\Omega H(\phi_i) dx dy - V_i^0 \right) \Bigg] \delta(\phi_i) \quad (2)$$

where

$$c_{I,i}(t) = \langle H(\phi_i) \rangle ; \quad c_O(t) = \left\langle \prod_j (1 - H(\phi_i)) \right\rangle \quad (3)$$

A shortcoming of Dufour's VCC is that the resultant shrinking or expanding force applies not only on the portion of cell boundary where the cell touches or resides inside another cell, but also on the whole boundary of a cell. Therefore, undesirable shrinkage or expansion may be caused on the whole cell boundary. For isolated cells, the image dependent terms—the second and third terms on the right side of Eq. (1), are sufficient for correct segmentation. Cells and nuclei change their shapes dramatically during cell division. When tracking cell mitosis events applying Dufour's approach, one may obtain inaccurate results due to such effects of the VCC term.

### 2.2 Four-coupled level sets

To reduce computational costs for segmenting of $N$ objects, a four-color level set (4LS) algorithm based on graph vertex coloring was presented in [16]. The authors use the Delaunay graph to capture spatial relationship of cells, with each vertex of the graph representing a cell. By applying a vertex coloring processing on the graph, each vertex is tagged with a color which is different from those of its adjacent vertices in the graph. Therefore, cells can be divided into groups, according to the colors assigned to them. Since cells in the same group/color are not adjacent spatially, one can assign a single level set function to handle the processing of all cells with the same color tag. The famous "four-color theorem" states that any planar graphs can be colored with at most four colors and no two neighboring vertices are assigned with the same color [18]. Hence, one requires only four level set functions and six coupling constraint terms for the processing of $N$ cells. This dramatically reduces the computational cost.

The four evolution equations are as follows ($i = 1, 2, 3, 4$):

$$\frac{\partial \phi_i}{\partial t} = \Bigg[\alpha \nabla \cdot \frac{\nabla \phi_i}{|\nabla \phi_i|} - \lambda_I (I - c_{I,i})^2 + \lambda_O \prod_{j=1, j \neq i}^{4} (1 - H(\phi_j)) (I - c_O)^2 - \gamma \sum_{j=i+1}^{4} H(\phi_j) \Bigg] \delta(\phi_i) + \zeta \left[ \Delta \phi_i - \nabla \cdot \frac{\nabla \phi_i}{|\nabla \phi_i|} \right] \quad (4)$$

where the last term enforces the constraint of $|\nabla\phi_i| = 1$.

In addition to the pair-wise coupling constraint weighted by $\gamma$ in Eq. (4), they also used an explicit coupling rule during the narrow-band evolution to penalize overlaps between level sets: a pixel on the front of a current level sets ($\delta(\phi_i) > s_{thresh}$) is updated only if its saliency is highest among all four level sets, i.e. $\delta(\phi_i) > \delta(\phi_j)$, for given $i$ and for all $j \neq i$.

## 3 Methodology

This section describes in detail our segmentation/clump separating method and three-color coupled level set (3LS) algorithm for cell tracking.

The main steps of the proposed segmentation and tracking algorithm are summarized as follows:

1) Segment the first frame of the sequence using Chan and Vese's two-phase level set algorithm [17].
2) Determine the cell number and positions by extracting concave points and performing ellipse fitting after initial segmentation. Produce a label map where each cell is represented by a unique label.
3) Use the label map to initialize three level set functions based on vertex coloring result.
4) Update $c_{I,i}$ and $c_O$ and evolve each level set function according to Eq. (11) until convergence.
5) Determine whether there are new objects entering the current frame by applying two-phase level set algorithm.
6) If there is a next frame, obtain a label map from the converged level set functions and go to step 3. Otherwise stop the algorithm.

We elaborate essential components of the algorithm as follows.

### 3.1 Concave Point Extraction and Ellipse Fitting

In level set based tracking methods, a good segmentation of the first frame is very important to perform correct tracking as it provides the information about the positions and the number of objects to be tracked [15]. At the beginning of our method, the first frame is binarized by Chan and Vese's approach [17] of active contours without edges in the level-set framework. Such initial segmentation tends to group close/touching cells together. Next, we use the derived *concave* points and ellipse fitting to separate clumped cells. Our concave point extraction and ellipse fitting method uses three parameters ($d$, $h_{\min}$, and $f_{\text{th}}$), comparing to Bai's popular method using seven parameters [19]. Let $\mathcal{B}$ be the binary image obtained. The output exterior boundaries of $\mathcal{B}$ are used to extract concave points. Let $p_c(x_c, y_c)$ be the point at order index $c, c = 1, 2, ..., N$ in a sequence of ordered points on a close boundary. $\theta(p_c)$, the degree of concavity of

$p_c$ is measured by the angle between the two vectors defined by three consecutive points $(p_{c-1}, p_c, p_{c+1})$:

$$\theta(p_c) = \begin{cases} a(p_{c-1}, p_c) - a(p_{c+1}, p_c), & \text{if } a(p_{c-1}, p_c) - a(p_{c+1}, p_c) > 0 \\ a(p_{c-1}, p_c) - a(p_{c+1}, p_c) + 2\pi, & \text{else} \end{cases} \quad (5)$$

where

$$a(p_{c-1}, p_c) = \arctan(y_{c-1} - y_c, x_{c-1} - x_c) \quad (6)$$

$$a(p_{c+1}, p_c) = \arctan(y_{c+1} - y_c, x_{c+1} - x_c) \quad (7)$$

The concave points are the local maxima of $\theta(p_c), c = 1, 2, ..., N$, with minimum peak separation distance of $d$ and minimum peak height of $h_{\min}$.

$$p_{\text{concave}} = \{p_{c^*} | \theta(p_{c^*}) \geq \theta(p_c) \quad \forall \quad |c - c^*| \leq d \text{ and } \theta(p_{c^*}) \geq h_{\min}\} \quad (8)$$

where $d$ is minimum peak separation distance and $h_{\min}$ are the minimum peak height. $d$ and $h_{\min}$ are pre-set thresholds. In the next step, the exterior boundaries are separated into contour segments by concave points. Note that if initial segmentation generates interior boundaries, *convex* points can be extracted by finding local minima of $\theta(p_c)$ in a similar way, then the interior boundaries can be separated into contour segments by convex points, which are crucial to separate a highly compact clump of cells.

The contour segments are fitted to ellipses using the least squares criterion. We define a score measuring the fitness between contour segment(s) $L$ and its fitted ellipse $\mathcal{E}(L)$ as follows

$$\text{fit}(L, \mathcal{E}) = \frac{\text{length}(L)}{\pi\sqrt{2(a^2 + b^2)}} \left(\frac{\text{area}(\mathcal{E} \cap \mathcal{B})}{\pi ab}\right)^3 \quad (9)$$

where $a$ and $b$ are the semi-major and semi-minor axes of $\mathcal{E}$, respectively. The first fraction on the right side is the ratio between the length of $L$ and the (approximated) perimeter of $\mathcal{E}$. In case $L$ consists of multiple contour segments, its length is the sum of those of all segments. The second fraction (in the bracket with cubic power) is the ratio of the area of the region enclosed by both $\mathcal{B}$ and $\mathcal{E}$ over the area of $\mathcal{E}$. For each connected component in $\mathcal{B}$, each single contour segment is fitted by an ellipse. If the fitness score is higher than a threshold $f_{\text{th}}$, then the segment matches the ellipse and such an ellipse is kept. Those unmatched segments are paired with each other to find the best fitted ellipse among all combinations, requiring fit $> f_{\text{th}}$. Let $L_i, i = 1, 2, ..., M$ be the unmatched segments from the same connected components. The procedure of segment combination is given in Algorithm 1. Fig. 1 illustrates the extracted concave points and ellipses fitted.

### 3.2 Graph Construction and Vertex Coloring

Instead of assigning a unique level set to every cell as [11] and [1], we aim to use a minimum number of level sets for the segmentation and tracking of the same

(a) (b) (c)

**Fig. 1.** (a) Original image with multiple touching cells. (b) Binary image and concave points. (c) Fitted ellipses: red ellipses are fitted to a single contour segment and blue ellipses are fitted to a pair of segments.

**for** $i = 1$ *to* $M$ **do**
  **for** $j = i + 1$ *to* $M$ **do**
    $L_{ij} = L_i \cup L_j$;
    Fit an ellipse $E_{ij}$ by using all the points on $L_{ij}$;
    $F(i, j) = \text{fit}(L_{ij}, E_{ij})$;
  **end**
**end**
$(i^*, j^*) = \arg\max_{i,j \in \{1,2,\ldots,M\}} F(i, j)$;
$f_{\max} = F(i^*, j^*)$;
**while** $f_{\max} > f_{\text{th}}$ **do**
  Keep $E_{i^* j^*}$;
  $F(i^*, j) = 0$, for $j = 1$ to $M$;
  $F(i, j^*) = 0$, for $i = 1$ to $M$;
  $(i^*, j^*) = \arg\max_{i,j \in \{1,2,\ldots,M\}} F(i, j)$;
  $f_{\max} = F(i^*, j^*)$;
**end**

**Algorithm 1:** Segment combination for ellipse fitting

number of cells. This problem can be solved by vertex coloring, a way of coloring the vertices of a graph such that no two adjacent vertices share the same color.

We construct a graph from the fitted ellipses as follows:

1) Generate a planar graph by applying Delaunay triangulation on the centroids of all ellipses/cells.
2) If the length of an edge derived from the triangulation is larger than a pre-set threshold $d_{\text{e}}$, the edge is removed from the graph.
3) Add a vertex which represents the background and add an un-directed edge between the background vertex and every other cell vertexes (it is reasonable to assume that every cell is touching with the background).

After the graph is built, we apply Brèlaz's DSATUR algorithm [20] to assign a color tag to each vertex so that no adjacent vertices are assigned with the same color tag. The background vertex in the graph we constructed is adjacent to every cell vertices; it will be assigned a color which is different from all cell vertices. By initializing one level set function with the ellipses tagged with the

same color, we need only three level set functions to represent the cells in our 2D segmentation and tracking problem.

If touching cells form a circle, the background inside the circle is assigned with another vertex and edges will be added between this vertex and the vertices of surrounding cells. Hence this vertex will be assigned with a color different from vertices of surrounding cells (but likely to be the same colors as other backgrounds).

Note that two vertexes might be adjacent in the graph even though their corresponding ellipses are not touching or overlapping. Two ellipses will be assigned to different colors if their distance is below a parameter $d_e$. This is to prevent them from merging in the subsequent frames. Here we assume each individual cell will overlap respectively in any two consecutive image frames. We empirically set $d_e$ to be 1.2 times the sum of the long axes of two ellipses.

The above method for graph construction and vertex coloring can be easily extended to the representation of cell relationship for the task of 3D cell segmentation. In this case, the vertices have three coordinate elements and edges are positioned in a 3D $(X, Y, Z)$ space instead of a 2D space. Therefore, the Delaunay triangulation and the edge length measurement need to be done in the 3D space. An example of such a graph is displayed in Fig. 2.

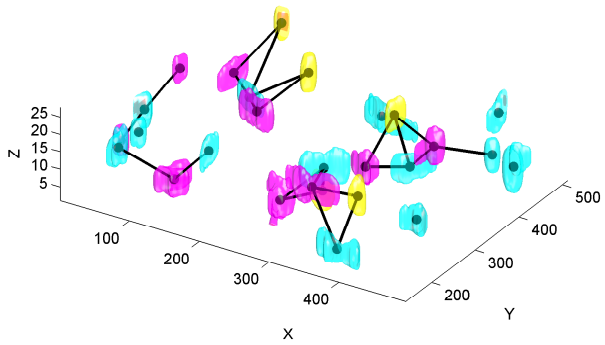


**Fig. 2.** A graph representing 3D cell relationship with vertices (in dots) and edges (in solid lines).

### 3.3 Three-color Coupled Level Sets

Our three-color coupled level sets algorithm is implemented in the nLS [1] framework to handle overlapped cells. To avoid the shrinkage or expansion on whole cell boundary caused by its VCC term, we propose an improved VCC which combines with a pair-wise coupling term. Our energy functional is defined with

three level set functions:

$$E(\phi_1,\phi_2,\phi_3,c_O,c_{I,1},c_{I,2},c_{I,3}) = \iint_\Omega \sum_{i=1}^{3}\Bigg[\alpha\delta(\phi_i)|\nabla\phi_i| + \lambda_I H(\phi_i)(I-c_{I,i})^2 + \frac{\lambda_O}{3}\prod_{j=1}^{3}\left(1-H(\phi_j)\right)(I-c_O)^2 + \gamma\sum_{j=i+1}^{3}H(\phi_i)H(\phi_j) + \frac{1}{2}\eta_i\sum_{q=1}^{N_i}\left(\left(\iint_\Omega H(\phi_{i,q})dxdy - V_{i,q}^0\right)^2\sum_{j=1,j\neq i}^{3}H(\phi_{i,q})H(\phi_j)\right)\Bigg]dxdy \quad (10)$$

where $N_i$ is the number of cells represented by $\phi_i, i = 1,2,3$ and $\phi_{i,q}$ is the level set function computed from the $q$th individual cell in $\phi_i$, $q = 1,2,...,N_i$. $N_i$ is determined in the vertex coloring procedure described in Section 3.2. As a result, the penalty of VCC (the term weighted by $\eta_i$ in Eq. (10) only applies to the part of cell boundary which touches or locates inside another cell. This VCC term disappears automatically on isolated cells which do not overlap with other cells. Three evolution equations ($i = 1,2,3$) can be derived by applying Euler-Lagrange equations to Eq. (10):

$$\frac{\partial\phi_i}{\partial t} = \Bigg[\alpha\nabla\cdot\frac{\nabla\phi_i}{|\nabla\phi_i|} - \lambda_I(I-c_{I,i})^2 + \lambda_O\prod_{j=1,j\neq i}^{3}\left(1-H(\phi_j)\right)(I-c_O)^2 - \gamma\sum_{j=i+1}^{3}H(\phi_j)\Bigg]\delta(\phi_i) - \eta_i\sum_{q=1}^{N_i}\Bigg[\left(\iint_\Omega H(\phi_{i,q})dxdy - V_{i,q}^0\right)\sum_{j=1,j\neq i}^{3}H(\phi_{i,q})H(\phi_j) + \frac{1}{2}\left(\iint_\Omega H(\phi_{i,q})dxdy - V_{i,q}^0\right)^2\sum_{j=1,j\neq i}^{3}H(\phi_j)\Bigg]\delta(\phi_{i,q}) \quad (11)$$

In Fig. 3, we illustrate the tracking results on two consecutive frames by coupled level sets. At $T_0$, only two level set functions are required for the segmentation due to the small cell number. At $T_1$, the coupled level sets without VCC fail to track the correct boundaries because of the lack of intensity difference between cells. Dufour's method causes the whole cell boundary to shrink (purple cell) or expand (blue cell) (Fig. 3(c)). Our method, which uses an improved VCC term, generates satisfactory result (Fig. 3(e)).

### 3.4 Tracking Scheme

Now we describe our tracking scheme used in this work. In the first frame of a temporal sequence, the cell number and positions are determined by extracting concave points and ellipse fitting after initial segmentation. Then, the cells/ellipses are used to initialize three level set functions based on the result of vertex coloring. Three-color coupled level sets without VCC is applied to segment the cell boundary. To process frames in subsequent times, the evolution

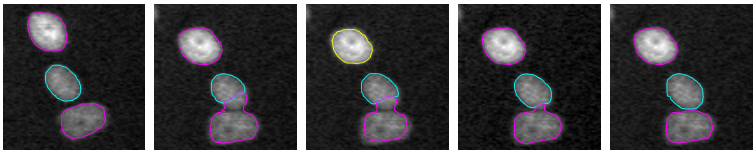

(a) (b) (c) (d) (e)

**Fig. 3.** Tracking results of coupled level sets. Contours of different color are represented by different level set functions. (a) Without VCC at $T_0$. (b) Without VCC at $T_1$. (c) Using Dufour's VCC at $T_1$. (d) Using Nath's explicit coupling rule without VCC at $T_1$. (e) Using our improved VCC at $T_1$.

result of Eq. (11) on the current frame is used to initialize the level set functions in the following frame. After each iteration, the distance between cells needs to be re-calculated. Cells within the distance threshold $d_e$ need to change to different colors (and to re-initialize the level sets) to prevent the merge of cells of the same color.

## 4 Experiments

### 4.1 Validation datasets

Our proposed method was tested on four publically available datasets. They are real time-lapse fluorescent microscopic image sequences, three in 2D (Hela1 [21], N2DL-Hela [22], and C2DL-MSC [22]) and one in 3D (C3DL-MDA231 [22]). The imaging acquisition setup of each dataset is listed in Table 1 [23]. Commonly used in cell population studies, the Hela1 and N2DL-Hela datasets are nuclear-stained (only nuclei are seen in the images). The two Hela datasets have high cell density and low resolution, some with very low fluorescent densities. Moreover, colliding, mitosis, entering and leaving cells are frequently present. The other two datasets, C2DL-MSC and C3DL-MDA231, are cytoplasm-stained. They are more appropriate for studies of single-cell morphology changes. The challenges in analyzing the C2DL-MSC dataset are the low signal-to-noise ratio and the presence of filament-like protrusions which often collide with each other. It is most difficult to process images in the 3D C3DL-MDA231 dataset: in addition to the colliding elongated cells, the data were acquired under high-throughput conditions (i.e., very low resolution in axial direction (difficult for segmentation) and very large time step (difficult for tracking)).

### 4.2 Evaluation metrics

During ellipse fitting, the parameters were fixed: $d = 5$, $h_{\min} = 3.9$, and $f_{\text{th}} = 0.5$. During evolution of the coupled level sets, the parameters were fixed to: $\alpha = 65$, $\lambda_I = 0.5$, $\lambda_O = 1$, $\gamma = 0$, $\eta = 2$, and the number of iterations for each frame is 50.

**Table 1.** Acquisition parameters and properties of the datasets.

| Dataset | Hela1 | N2DL-Hela | C2DL-MSC | C3DL-MDA231 |
|---|---|---|---|---|
| Objective | | Plan 10x/0.4 | Plan-Neofluar 10x/0.3 | Plan 20x/0.7 |
| Frame size | 672×512 | 1100×700 | 992×832 | 512×512×30 |
| Pixel size ($\mu$m) | | 0.645×0.645 | 0.3×0.3 | 1.242×1.242×6 |
| Time step | 15 min | 30 min | 20 min | 80 min |
| No. of frames | 25 | 30 | 48 | 12 |
| No. of moves | 1444 | 760 | 413 | 331 |
| No. of divisions | 15 | 29 | 0 | 0 |

The segmentation results of the proposed three-color coupled level sets (3LS) were compared against the ground truth which is the consensus of three human experts, in terms of precision, recall, and F-score. Following the evaluation method in [23], a reference cell in ground truth and a segmented one are considered matching if their overlapping area is more than 50% of the total area of the reference cell. Therefore, for each reference cell, there can be one matching segmented cell at most. In case there is no segmented cell matching with the reference cell, the three segmentation accuracy indices are set to zero. The segmentation accuracy is calculated as the mean of all the reference cells in the sequence, including these zeros. The percentage of matched reference cells is also computed. When we vary $d \in [1, 32]$, $h_{\min} \in [3.6, 4.2]$, $f_{\text{th}} \in [0.4, 0.7]$, the precision, recall, and F-score of the first frame of Hela1 are $0.972 \pm 0.006$, $0.914 \pm 0.008$, and $0.921 \pm 0.006$ respectively. The result shows that the segmentation accuracy is not sensitive to the parameters. The tracking accuracy was measured by the successful detection rate in move events and division events. A move event refers to one cell moving from one frame to the next (no division happens) or newly appears in a frame.

### 4.3 Numerical results

We choose to compare the performance of our algorithm with the n-coupled level sets (nLS) [1,11], the four-coupled level sets (4LS) [16], and a publicly available software: DCellIQ [21] based on [24] and [25], which adopts a "detection and then linking" strategy. We use our segmentation result from the first frame to initialize the $n$ level set functions in nLS and the four level set functions in 4LS. Examples of segmentation results are shown in Fig. 4 and Fig. 5.

The quantitative evaluation results are shown in Tables 2-5. 3LS's segmentation accuracy and tracking accuracy are notably higher than those of DCellIQ and nLS in all four datasets. For the Hela1 dataset, all method perform well in finding matched reference cells ('match' in Table 2) and achieve high recall of segmentation. DCellIQ and nLS perform poorer in the segmentation precision than 4LS and 3LS. 3LS is significantly better than DCellIQ, nLS and 4LS in tracking of cells in divisions. For the N2DL-Hela dataset, all accuracy measures

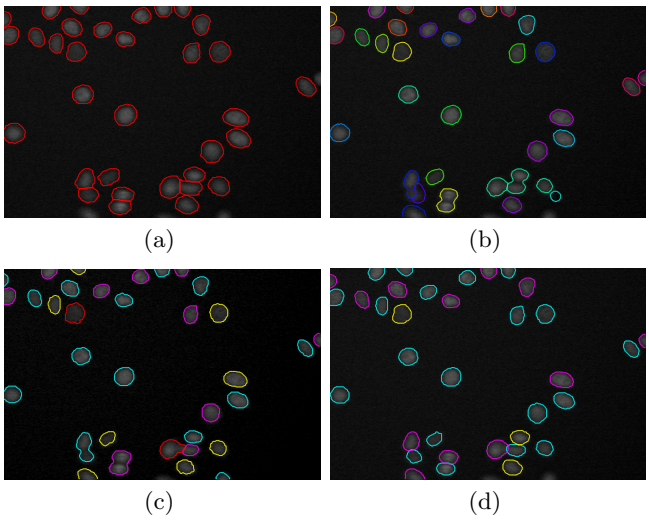

**Fig. 4.** Segmentation results on Hela1 dataset from (a) DCellIQ, (b) nLS, (c) 4LS, and (d) 3LS.

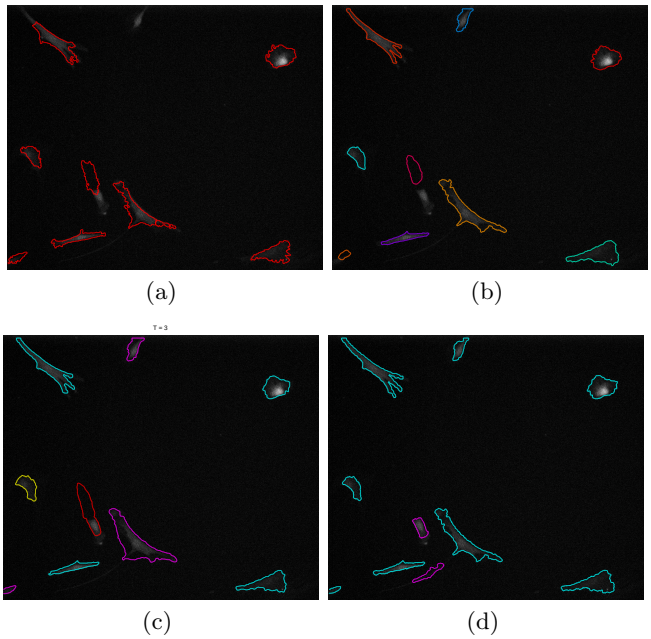

**Fig. 5.** Segmentation results on C2DL-MSC dataset from (a) DCellIQ, (b) nLS, (c) 4LS, and (d) 3LS.

are lower (Table 3), due to the fact that this sequence contains more nuclei of low intensity which are difficult for these two-phase level set based methods to detect. 3LS shows slight improvement of accuracy over 4LS on the two Hela datasets.

For the C2DL-MSC dataset, 3LS outperforms 4LS by around 15% in both segmentation accuracy and tracking accuracy (Table 4). As a narrow-band approach, 4LS may be difficult to track drastically changed cell shapes across frames. Besides, its explicit topological coupling constraint can prevent false merging or absorption of neighboring cells; However, it lacks of a VCC term to handle touching cells smartly by making use of the area/volume information from the previous frame. For the C3DL-MDA231 dataset, a roughly 20% increase in segmentation accuracy is achieved by 3LS (Table 5). Overall, 3LS is the most accurate method among the four methods under test.

**Table 2.** Segmentation and tracking accuracy on Hela1 dataset.

| | Segmentation | | | | Tracking | |
|---|---|---|---|---|---|---|
| Method | precision | recall | F-score | match | move | division |
| DCellIQ | 0.727 ± 0.158 | 0.967 ± 0.167 | 0.825 ± 0.158 | 97.3 % | 83.9 % | 46.7 % |
| nLS | 0.769 ± 0.200 | 0.947 ± 0.179 | 0.838 ± 0.183 | 97.0 % | 94.9 % | 33.3 % |
| 4LS | 0.857 ± 0.186 | 0.932 ± 0.162 | 0.885 ± 0.166 | 97.8 % | 92.7 % | 46.7 % |
| 3LS | 0.840 ± 0.165 | 0.951 ± 0.162 | 0.887 ± 0.156 | 97.5 % | 96.9 % | 73.3 % |

**Table 3.** Segmentation and tracking accuracy on N2DL-Hela dataset.

| | Segmentation | | | | Tracking | |
|---|---|---|---|---|---|---|
| Method | precision | recall | F-score | match | move | division |
| DCellIQ | 0.514 ± 0.362 | 0.596 ± 0.408 | 0.543 ± 0.373 | 70.0 % | 64.1 % | 75.9 % |
| nLS | 0.613 ± 0.403 | 0.682 ± 0.415 | 0.635 ± 0.399 | 74.2 % | 76.1 % | 34.5 % |
| 4LS | 0.718 ± 0.419 | 0.664 ± 0.387 | 0.684 ± 0.394 | 75.8 % | 77.0 % | 79.3 % |
| 3LS | 0.705 ± 0.393 | 0.710 ± 0.399 | 0.700 ± 0.387 | 74.2 % | 78.0 % | 79.3 % |

The computational time per iteration of nLS and 3LS are compared in Table 6. Without VCC, i.e., the $\eta_i$ term in Eq. (1) and Eq. (10), the 3LS's computational time is only 3% of the nLS's in the 2D image and 8% in the 3D image. With the VCC term, the 3LS's computational time is 5% of nLS's in 2D and 17% in 3D. This is because 3LS reduces the number of coupling terms from $O(N^2)$ to $O(1)$ for $N$ objects. Comparing with the 4LS, the computational time of 3LS without VCC has also been reduced by 30%.

**Table 4.** Segmentation and tracking accuracy on C2DL-MSC dataset.

| | Segmentation | | | | Tracking | |
|---|---|---|---|---|---|---|
| Method | precision | recall | F-score | match | move | division |
| DCellIQ | 0.646 ± 0.415 | 0.430 ± 0.313 | 0.505 ± 0.341 | 65.2 % | 60.1 % | - |
| nLS | 0.589 ± 0.444 | 0.436 ± 0.347 | 0.493 ± 0.377 | 64.3 % | 73.9 % | - |
| 4LS | 0.584 ± 0.411 | 0.476 ± 0.343 | 0.513 ± 0.358 | 68.8 % | 79.2 % | - |
| 3LS | 0.754 ± 0.340 | 0.604 ± 0.289 | 0.663 ± 0.301 | 83.9 % | 95.6 % | - |

**Table 5.** Segmentation and tracking accuracy on C3DL-MDA231 dataset.

| | Segmentation | | | | Tracking | |
|---|---|---|---|---|---|---|
| Method | precision | recall | F-score | match | move | division |
| nLS | 0.428 ± 0.354 | 0.572 ± 0.401 | 0.460 ± 0.342 | 70.0 % | 86.1 % | - |
| 4LS | 0.570 ± 0.434 | 0.524 ± 0.380 | 0.528 ± 0.387 | 67.5 % | 89.1 % | - |
| 3LS | 0.685 ± 0.283 | 0.782 ± 0.289 | 0.714 ± 0.267 | 90.0 % | 91.8 % | - |

## 5 Conclusions

In this paper, a new algorithm for cell segmentation and tracking is proposed based on the coupled active contour framework. Two new solutions were presented to address the shortcomings of the original relevant algorithms. Specifically, we use only three level set functions to segment and track arbitrary number of cells in the image sequences, taking advantage of a vertex coloring approach in image graph representations. Also, we redefine the volume conservation constraint in the optimization functional. This is to reduce the undesirable shrinkage or expansion caused on the whole cell boundary. In addition, we develop an algorithm for touching cell separation in image segmentation, based on concave points and ellipse fitting. Experimental results show improved segmentation performance of our new algorithm, as well as tracking performance in terms of successful detection rates in move events and division events. Finally, the computational time of the new algorithm is notably reduced compared with the original n-coupled level set algorithm.

**Table 6.** Computational time (sec) per iteration.

| | 2D (Hela1, 72 cells) | | 3D (C3DL-MDA231, 31 cells) | |
|---|---|---|---|---|
| Method | w/o VCC | with VCC | w/o VCC | with VCC |
| nLS | 13.1 | 13.4 | 152 | 154 |
| 4LS | 0.51 | - | 17.2 | - |
| 3LS | 0.36 | 0.68 | 12.1 | 26.5 |

## References


1. Dufour, A., Shinin, V., Tajbakhsh, S., Guillen, N., Olivo-Marin, J.C., Zimmer, C.: Segmenting and tracking fluorescent cells in dynamic 3-D microscopy with coupled active surfaces. IEEE Trans. Image Processing **14** (2005) 1396–1410
2. Zimmer, C., Zhang, B., Dufour, A., Thebaud, A., Berlemont, S., Meas-Yedid, V., Marin, J.C.O.: On the digital trail of mobile cells. IEEE Signal Processing Magazine **23** (2006) 54–62
3. Zhou, X., Yang, J., Wang, M., Wong, S.T.C.: A novel cell tracking algorithm and continuous hidden markov model for cell phase identification. In: IEEE/NLM Life Science Systems and Applications Workshop, Bethesda, MD (2006) 1–2
4. Chen, X., Zhou, X., Wong, S.: Automated segmentation, classification, and tracking of cancer cell nuclei in time-lapse microscopy. IEEE Trans. Biomedical Engineering **53** (2006) 762–766
5. Zhou, X., Li, F., Yan, J., Wong, S.T.C.: A novel cell segmentation method and cell phase identification using markov model. IEEE Trans. Information Technology in Biomedicine **13** (2009) 152–157
6. Li, F., Zhou, X., Ma, J., Wong, S.T.C.: Multiple nuclei tracking using integer programming for quantitative cancer cell cycle analysis. IEEE Trans. Medical Imaging **29** (2010) 96–105
7. Hu, Y., Osuna-Highley, E., Hua, J., Nowicki, T.S., Stolz, R., McKayle, C., Murphy, R.F.: Automated analysis of protein subcellular location in time series images. Bioinformatics **26** (2010) 1630–1636
8. Harder, N., Mora-Bermdez, F., Godinez, W.J., Ellenberg, J., Eils, R., Rohr, K.: Automated analysis of the mitotic phases of human cells in 3D fluorescence microscopy image sequences. Lecture Notes in Computer Science (MICCAI) **4190** (2006) 840–848
9. Yang, X., Li, H., Zhou, X.: Nuclei segmentation using marker-controlled watershed, tracking using mean-shift, and kalman filter in time-lapse microscopy. IEEE Tran. Circuits and Systems I **53** (2006) 2405–2414
10. Zimmer, C., Labruyere, E., Meas-Yedid, V., Guillen, N., Olivo-Marin, J.C.: Segmentation and tracking of migrating cells in videomicroscopy with parametric active contours: A tool for cell-based drug testing. IEEE Trans. Medical Imaging **21** (2002) 1212–1221
11. Zhang, B., Zimmer, C., Olivo-Marin, J.C.: Tracking fluorescent cells with coupled geometric active contours. In: Proc. IEEE Int'l Symp. Biomedical Imaging (ISBI). (2004) 476–479
12. Mukherjee, D., Ray, N., Acton, S.: Level set analysis of leukocyte detection and tracking. IEEE Trans. Image Processing **13** (2004) 562–572
13. Yang, F., Mackey, M., Ianzini, F., Gallardo, G., Sonka, M.: Cell segmentation, tracking, and mitosis detection using temporal context. Lecture Notes in Computer Science (MICCAI) **3749** (2005) 302–309
14. Padfield, D., Rittscher, J., Thomas, N., Roysam, B.: Spatio-temporal cell cycle phase analysis using level sets and fast marching methods. Medical Image Analysis **13** (2009) 143–155
15. Dzyubachyk, O., Van Cappellen, W.A., Essers, J., Niessen, W.J., Meijering, E.: Advanced level-set based cell tracking in time-lapse fluorescence microscopy. IEEE Trans. Medical Imaging **29** (2010) 852–867
16. Nath, S.K., Palaniappan, K., Bunyak, F.: Cell segmentation using coupled level sets and graph-vertex coloring. Lecture Notes in Computer Science (MICCAI) **4190** (2006) 101–108

17. Chan, T.F., Vese, L.A.: Active contours without edges. IEEE Trans. Image Processing **10** (2001) 266–277
18. Thomas, R.: An update on the four-color theorem. Notices of the AMS **45** (1998) 848–859
19. Bai, X., Sun, C., Zhou, F.: Splitting touching cells based on concave points and ellipse fitting. Pattern Recogn. **42** (2009) 2434–2446
20. Brélaz, D.: New methods to color the vertices of a graph. Commun. ACM **22** (1979) 251–256
21. DCellIQ: The Dynamic Cell Image Quantitator software package. (http://www.cbi-tmhs.org/Dcelliq/index.html)
22. ISBI: The First Cell Tracking Challenge. (http://www.codesolorzano.com/celltrackingchallenge)
23. Maška, M., Ulman, V., Svoboda, D., Matula, P., Matula, P., Ederra, C., Urbiola, A., España, T., Venkatesan, S., Balak, D.M., Karas, P., Bolcková, T., X0160 Treitova, M., Carthel, C., Coraluppi, S., Harder, N., Rohr, K., Magnusson, K.E., Jaldén, J., Blau, H.M., Dzyubachyk, O., Krízek, P., Hagen, G.M., Pastor-Escuredo, D., Jimenez-Carretero, D., Ledesma-Carbayo, M.J., Muñoz-Barrutia, A., Meijering, E., Kozubek, M., Ortiz-de Solorzano, C.: A benchmark for comparison of cell tracking algorithms. Bioinformatics **30** (2014) 1609–1617
24. Li, F., Zhou, X., Zhu, J., Ma, J., Huang, X., Wong, S.T.: High content image analysis for human h4 neuroglioma cells exposed to cuo nanoparticles. BMC Biotechnology **7** (2007)
25. Wang, M., Zhou, X., Li, F., Huckins, J., King, R.W., Wong, S.T.C.: Novel cell segmentation and online svm for cell cycle phase identification in automated microscopy. Bioinformatics **24** (2008) 94–101